The spectroscopy of fission fragments

W.R. Philipps

THE SPECTROSCOPY OF FISSION FRAGMENTS

W.R.Phillips

Department of Physics and Astronomy,
University of Manchester, Manchester, M13 9PL, U.K.

RESUME

L'utilisation de multidétecteurs γ à haute résolution et grande sélectivité dans l'étude des raies γ émises par des fragments de fission a fourni un ensemble de données sur les noyaux riches en neutrons qui n'auraient pas pu être obtenues d'une autre façon. Les structures yrast et yrare de nombreux fragments de fission riches en neutrons ont été observées durant la dernière décennie. Ce papier décrit le champ d'études abordé, les techniques utilisées, ainsi que quelques résultats tirés d'expériences récentes.

ABSTRACT

High-resolution measurements on γ rays from fission fragments have provided a rich source of information, unobtainable at the moment in any other way, on the spectroscopy of neutron-rich nuclei. In recent years important data have been obtained on the yrast- and near yrast-structures of neutron-rich fission fragments. We discuss the scope of measurements which can be made on prompt gamma rays from secondary fission fragments, the techniques used in the experiments and some results recently obtained.

1. INTRODUCTION

Experiments made to study neutron-rich nuclei with as large a neutron excess as possible are performed on fragments produced in low-energy fission such as spontaneous fission or fission induced by low-energy neutron or proton beams. This is because at high excitations of the fissioning system more neutrons are emitted in the cooling down to secondary fragments than at low excitation. Fission at low energy usually gives rise to a characteristic double-humped mass distribution. The mass and charge distributions of the secondary fragments which can be studied are determined by the particular fission process and by the power of the gamma-ray detection array used in the experiments. Figure 1 shows a schematic picture of a particular mode of fission of the nucleus ^{248}Cm, and serves to define primary and secondary fragments as the terms are used in this paper.

Results discussed here were obtained using the EUROGAM array, and the techniques outlined were designed for use with that array although they are applicable to any similar detection equipment. This paper first discusses the scope of present measurements on secondary fragments from low-energy fission, showing the nuclei studied and the spin range over which discrete levels in these nuclei have been observed. Following that, the techniques

used to obtain level schemes, level lifetimes, to identify new nuclei and to obtain gamma-ray correlation and polarisation data are outlined. Finally some recent results obtained with EUROGAM2 are presented.

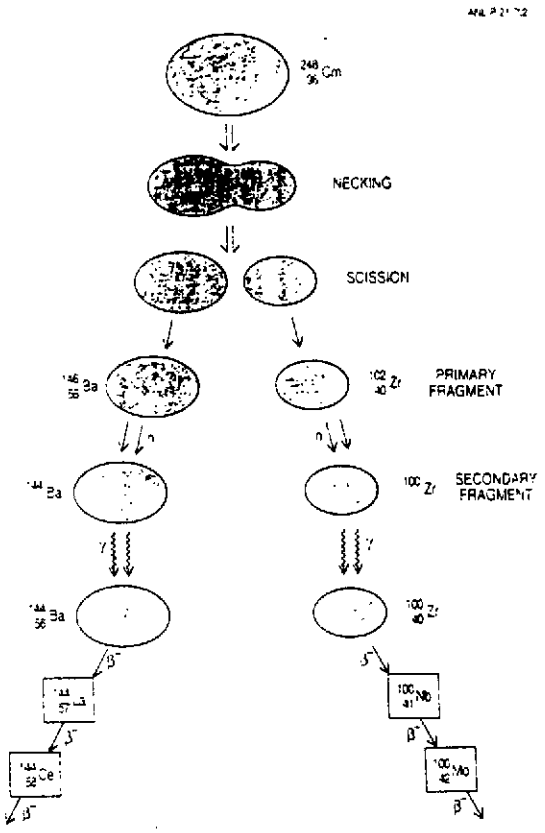

Figure 1. A schematic drawing showing a path to formation of a particular pair of secondary fragments. ^{144}Ba and ^{100}Zr, in the spontaneous fission of ^{248}Cm.

2. MASS, CHARGE AND SPIN DISTRIBUTIONS

The scope of spectroscopic studies is determined by the distribution of secondary fragments made in realisable fissioning systems and by the range of spins the fission mechanism produces in those fragments. Yields of different fission products depend on the mass and charge of the nucleus which fissions and on its excitation energy. In general, fission of the ground state of a nucleus with a large N/Z ratio produces the most neutron-rich nuclei. Spontaneous fission and thermal-neutron induced fission have double-humped mass distributions with two separate peaks centred close to masses 100 and 140. It has been found that the mean mass of the higher mass peak remains the same for low energy fission of actinide nuclei of different mass but the mean mass of the lower peak increases with increase in mass of the fissioning nucleus. Thus, yields of nuclei in the low-mass hump produced in the thermal neutron induced fission[1)] of ^{235}U are different from their yields in the spontaneous fission[2)] of ^{252}Cf.

For a given mass number $A = (N + Z)$ of a secondary, prompt γ-emitting fragment,

the most probable atomic number $Z_P(A)$ is given to a first approximation by

$$Z_P(A) = \frac{Z_f}{(A_f - \nu)} \times A.$$

where the subscript f refers to the fissioning nucleus and ν is the average number of neutrons emitted per fission. The charge distribution for a given A is given, to a good approxiation, by

$$P(A, Z) = \sigma_Z(2\pi)^{1/2}\exp[-(Z_P(A) - Z)^2/2\sigma_Z^2],$$

where σ_Z the dispersion is close to 0.5.

For a given atomic number of the secondary fragment the mass number distribution is also given by an expression of the above form with the mass dispersion σ_A about equal to $0.5\times(A_f/Z_f)$.

The spin distributions in fission fragments, together with the sensitivity of the detection equipment, determine the range of spins over which level stuctures in the fragments can be observed. The average spin in spontaneous fission fragments was known from early experiments [3,4] to be in the range 6-7$\hbar$. However, there is evidence that the spin distribution is skewed towards the high-spin side, and with the latest generation of γ-ray detector arrays it is possible to examine levels in strongly populated secondary fragments with spins up to $\sim 20\hbar$.

Normally fragments are formed hot at scission. A typical primary fragment may have an excitation energy of $\sim$ 20 MeV and a spin of $\sim 7\hbar$. It cools down with emission of two neutrons leaving a secondary fragment at excitation energy of a few MeV. The secondary fragment then continues to deexcite by γ-ray emission. The γ rays in the secondary fragment arise from a broad range of excitation energy corresponding to the spread in energies of the neutrons emitted from the primary fragment. They also arise from levels with a large spread of spins corresponding to the spread in the primary fragments introduced by the fission mechanism. There are also many γ-ray paths to the ground state from any point in this entry region. A variable number of *statistical* γ rays, with essentially continuous energy distribution and relatively high energies of an MeV or greater, takes the secondary fragment from the initial chaotic entry region down to a more ordered regime in which there are rather few yrast or near-yrast levels. This is illustrated schematically in figure 2. The number of statistical γ rays depends partly on the initial excitation energy of the primary fragment; in spontaneous fission there are typically one to three statistical γ rays per fragment.

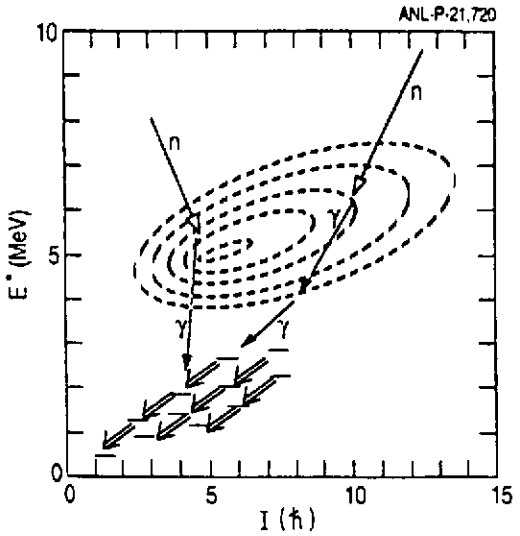

Figure 2. A schematic diagram illustrating a typical entry region into a secondary fragment.

Figure 3 shows the average spins $< I >$ of formation of discrete levels in fragments from three different fission processes. The data were obtained from direct analyses[5] of the intensities of the discrete γ rays. The figure shows that heavy-ion induced fusion-fission gives higher values of $< I >$ than low-energy fission, and should therefore allow the construction of level schemes up to higher spins. However, this advantage is outweighed by the disadvantages that (i) the mass ditributions are broadened, making it experimentally more difficult to examine in detail any one product, and (ii) the fragments are on average less neutron-rich than in low energy fission because more neutrons are emitted in total as pre-fission neutrons and/or from the more highly excited primary fragments.

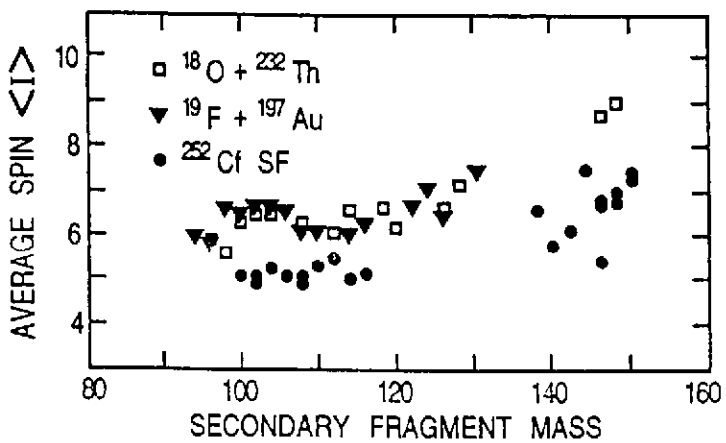

Figure 3. Average spins in secondary fission fragments.

3. EXPERIMENTAL TECHNIQUES

The chief difficulty when performing experiments on prompt γ rays from fission prod-

ucts is that many pairs of fragments are formed, each one typically emitting several γ rays. A particular nucleus under investigation needs a high degree of selectivity, and in prompt γ-ray experiments this is obtained by demanding time coincidences between (usually) three or more γ rays from the same fission event. Fragments come in pairs, and greater than 99% of pairs have $Z_1 + Z_2$ equal to Z_f. Gating on a known γ ray in a particular nucleus (A_1, Z_1) gives rise to coincident lines in several nuclei since there is a range of mass numbers A_2 accompanying Z_2. Although this complicates coincidence spectra, it can sometimes be helpful since it enables spectra containing (apart from impurities) only lines in two nuclei to be produced.

The usual techniques of γ-ray analysis are used to determine partial decay schemes in fragments. Triple coincidences are organised into three-dimensional arrays, each axis corresponding to energies deposited in a germanium detector. Gating on two axes enables spectra of coincident γ rays to be produced and used to build up decay patterns. The starting points are usually lines known from earlier work, often studies of mass isolated bets-decaying fission product ground dstates. When nuclei about which nothing was previously known have been examined their identification has been made by comparing the yields of complementary fragments: the average complementary fragment mass is a good signature of the mass of the new fragment studied [6,7].

The nearly 4π coverage of EUROGAM2 and the close arrangement of four individual germanium crystals in the 'clover' detectors used in that array have allowed the application of γ-ray correlation and polarization techniques to greatly increase the spectroscopic information obtained on fission fragments.

3.1 Directional Correlations

When prompt γ rays are observed in an array without observation of fragments, the first γ ray in a decay sequence arises from the decay of a state which is unaligned, i.e. equally populated amongst its magnetic substates. For a cascade of two γ rays the second is then distributed anisotropically with respect to the first and if the directional correlation is measured, information can be obtained on the spins of the levels involved in the transitions and on the multipolarities of the two γ rays. Measurements on double cascades as described above are of limited use because of the lack of selectivity when using only a single coincidence gate on a fission spectrum. If selected triple coincidences are observed, and the energy information stored in a three-dimensional data array (cube) two gates can be used to increase the resolving power. If the first axis of a cube containing triple coincidences corresponds to γ rays observed anywhere in the array, while the other two axes correspond to detectors with roughly the same angle θ between them, gating on the first axis for selectivity will (to a good approximation because of the near-isotropy of EUROGAM2) maintain the non-alignment of the top state in a cascade observed on the other axes. Cubes for detectors at different angles θ then allow the determination of the γ-γ directional correlation function. Figure 4 shows the validity of this approach as applied to cascades of known properties. For the cascades of two stretched electric quadrupoles (E2-E2) on the left-hand side of the figure the theoretical value of the coefficients A_{22}/A_{00}

and A_{44}/A_{00} are 0.102 and 0.009 respectively. For the stretched E1-E2 cascades on the right the theoretical values are -0.07 and zero respectively.

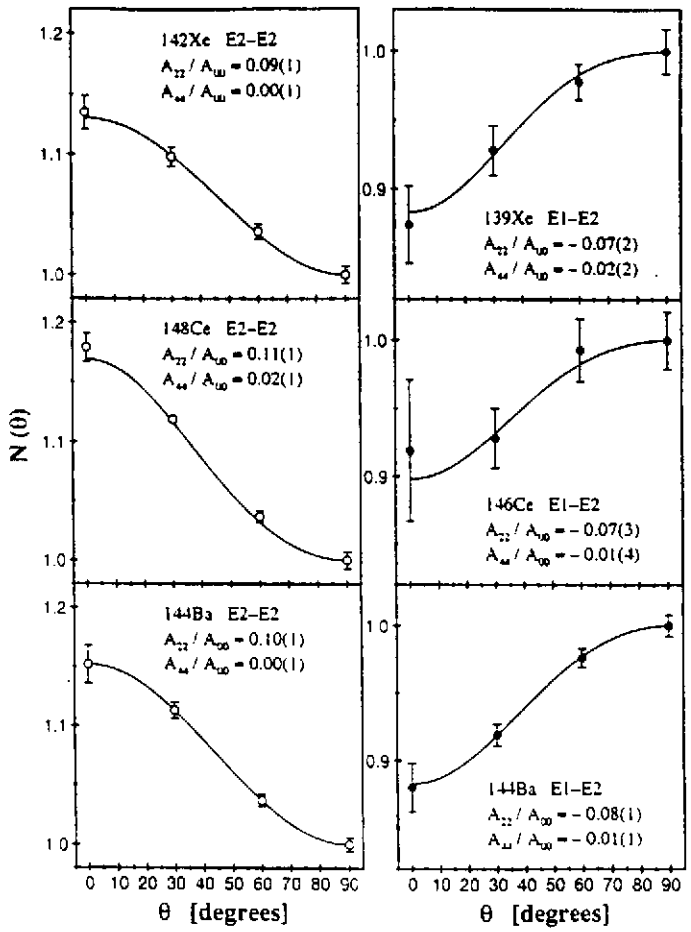

Figure 4. Observed $\gamma-\gamma$ directional correlations for stretched cascades as described in the text.

3.2 Polarizations

There is a higher cross section for Compton-scattering of a linearly polarized photon in a direction perpendicular to the plane containing the electric field vector and the momentum vector than there is in a direction parallel to that plane. The construction of the clover detectors in EUROGAM2 , in which four germanium crystals sit side by side forming a square, allows these detectors to be used as Compton polarimeters. The clovers are placed close to 90° to the beam direction and arranged such that scattering from one element to another either corresponds to scattering in the plane defined by the beam axis and the line joining the target to the clover detector, or scattering perpendicular to that plane.

In a γ_1-γ_2 cascade beginning on a state which is equally populated amongst its substates the probability of there being a coincidence event for two detectors with angle θ between them, and with Ψ the angle between the direction of the electric field vector and

the plane containing the momentum vectors of the two γ rays, is proportional to [8] the function

$$W(\gamma_2; t_1, t_2, \theta, \Psi) = \sum_{\lambda} \left(A_\lambda(t_1, t_2) P_\lambda(\cos\theta) + A_\lambda^{(p)}(t_1, t_2) P_\lambda^{(2)}(\cos\theta) \cos(2\Psi) \right).$$

where P_λ and $P_\lambda^{(2)}$ are Legendre polynomials and t_1 and t_2 label the properties of the two transitions and the states between which the transitions are made. The coefficients A depend upon the pathways t. If the detection system is insensitive to polarization, integrating over all angles Ψ gives the γ-γ directional correlation function discussed in Section 3.1.

If data are taken with γ_1 detected in Ge detectors close to zero or 180°, and γ_2 detected via summing scattered signals in two elements of a clover near 90° the experimental arrangement approximates that described in the opening paragraph of this section. For the angle Ψ equal to zero, the scattering parallel to the plane defined by the momentum vectors of γ_1 and γ_2 has a lower probability than that perpendicular to the plane, and vica versa if the angle Ψ equals $\pi/2$. The polarization of a beam of γ_2 photons detected in two elements of a clover in coincidence with γ_1 can be defined as

$$P = \frac{W(90, 90) - W(90, 0)}{W(90, 90) + W(90, 0)}.$$

Using equation (3.1) with θ equal to 90°, this can be calculated for given pathways t and depends on the electric and magnetic nature of the transition γ_2. It can be measured by observing the number of scattered events $N_\parallel$ and $N_\perp$ in appropriate elements of the clover detectors.

$$P = \left(\frac{N_\perp - N_\parallel}{N_\perp + N_\parallel} \right) \cdot \left(\frac{R+1}{R-1} \right).$$

Comparison of measurement with predictions then gives information on the multipolarity and parity of the transition γ_2. In the above formula R is a parameter depending on the different Compton scattering cross-sections at zero and 90°. For non-point detectors averaging over all angles involved gives

$$P = \frac{1}{Q} \cdot \frac{aN_\perp - N_\parallel}{aN_\perp + N_\parallel},$$

where Q is the polarization sensitivity of the polarimeters, obtained by calibration, and a is a factor close to unity which takes into account any instrumental anisotropy.

Figure 5 shows the validity of the polarization technique as applied to cascades of known properties in various nuclei. In spite of relatively large errors on the data they can still easily distinguish between transitions of pure electric or pure magnetic type because the two P values, although equal, have opposite sign.

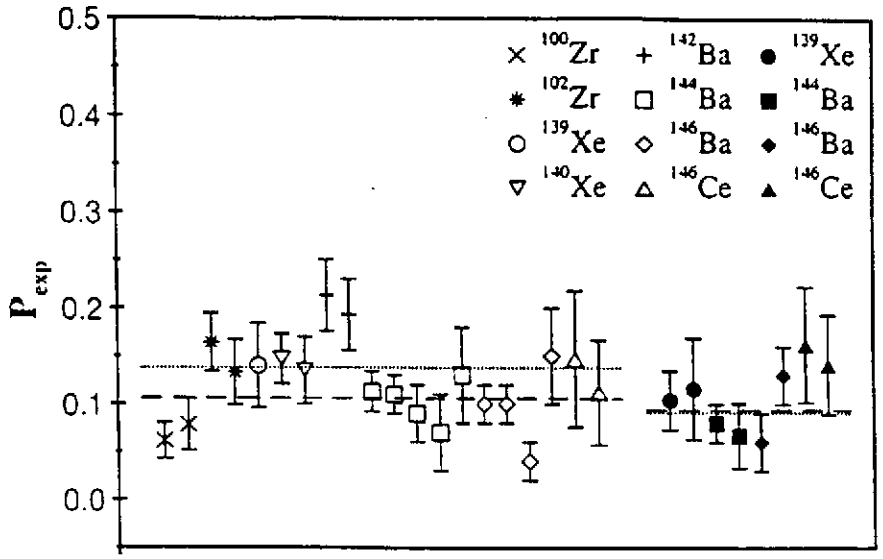

Figure 5. Observed polarisations for known stretched E2-E2 and E1-E2 cascades in fission fragments. Full symbols are E1-E2 and open are E2-E2. The horizontal dashed lines show averges of experimental values: the dotted lines show predictions.

3.3 Lifetimes

For a fission source uniformly embedded in a solid environment the fission fragments to a good approximation are all stopped in a very short time and with ranges of 3-15 mg cm^{-2} depending on the stopping material. The initial energy of a typical fragment from spontaneous fission is about 1 MeV per nucleon, and the range in gold of a fragment of this energy is typically about 13 mg cm^{-2} ($\sim 7 \times 10^{-4}$ cm) with a slowing down time of about 1.5 ps. For a source embedded in a material of lower average atomic number, the rate of energy loss per unit length is lower, the range in mg cm^{-2} somewhat lower and the slowing down time a little longer. If a secondary fragment emits a γ ray from a state with a lifetime shorter than the slowing down time, the energy of the γ ray is Doppler shifted by an amount depending on the speed of the fragment at the time of emission and the angle of emission of the γ ray with respect to the direction of motion of the fragment. For γ rays detected singly in an array without observation of the fragments the result is a symmetric broadening of the line shapes about the energies the γ rays would have if emitted from fragments at rest. For an approximately isotropic array γ rays observed in coincidences taken between all detectors also originate from unaligned states and the result is a similar broadening of the line shape. Observation of this broadening, and analyses made assuming knowledge of the slowing down process and of the manner in which the states are produced from the entry points into the secondary fragments, have been used [9] to measure lifetimes. The lineshapes must be extracted cleanly enough and the lifetimes must be comparable to the slowing down time for good results to be obtained. Figure 6 shows an example of fits to yrast transitions in Nd isotopes.

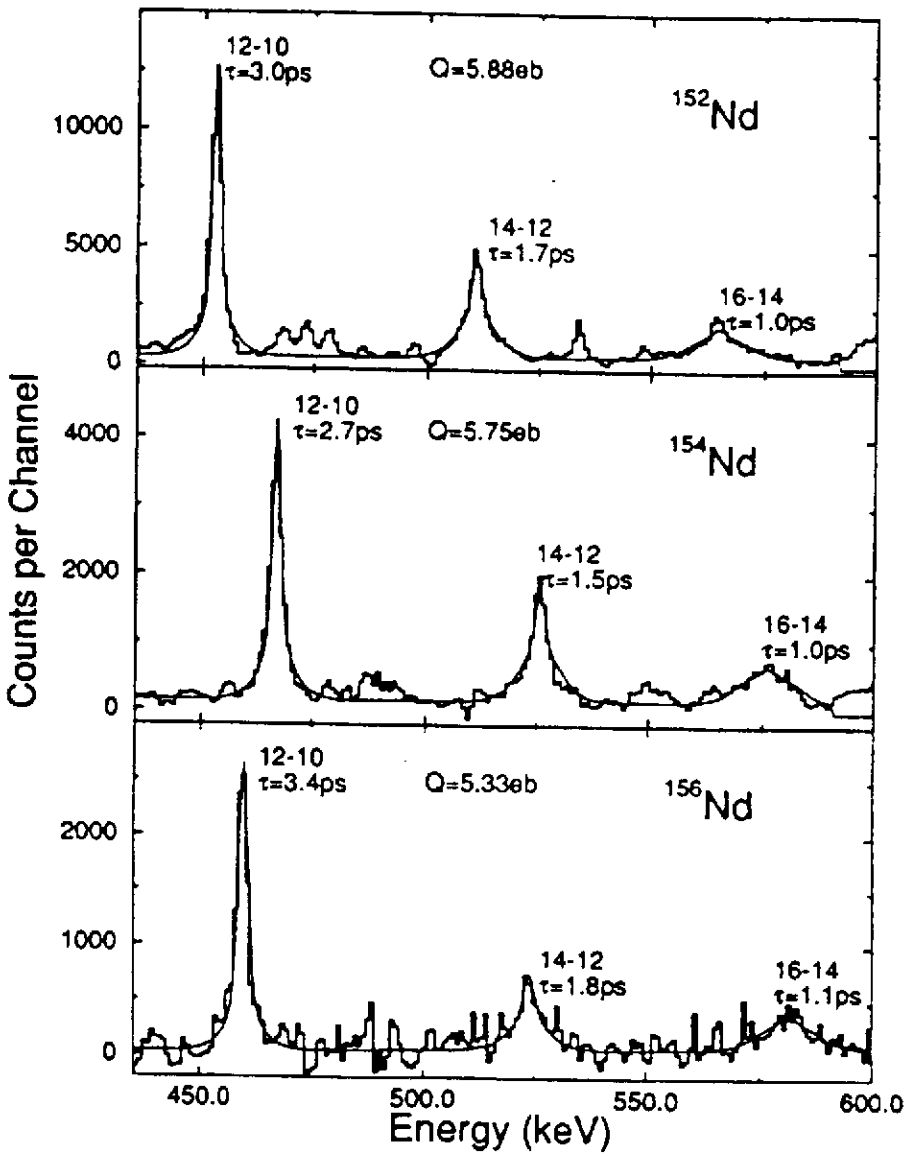

Figure 6. Line shapes in the γ-ray energy spectra of ^{152,154,156}Nd.

Lifetime measurements extracted in this way are subject to uncertainties due to lack of precise knowledge of stopping powers and to unknown details of feeding mechanisms. Relative lifetimes in an isotopic sequence, as in the case of the Nd isotopes above, are not subject to errors from stopping powers. The uncertainty arising from unknown feeding times can be reduced by including different models of the feeding process in the analysis. To the extent that such analyses give reasonable estimates of feeding times, they can be used to give valuable information on fragment formation-mechanisms as the neutron excess changes.

4. NEW SPECTROSCOPIC RESULTS

4.1 Octupole correlation effects in nuclei near mass 100

The structures at low excitation energy of neutron-rich nuclei near N=88 and Z=56 are expected to be influenced by strong octupole correlations. The close spacing of appropriate deformed single-particle orbits near the Fermi surface in this region may allow strong enough mixing of opposite parity states for the nucleus to be reflection-asymmetric in the intrinsic frame. Some time ago, features characteristic of octupole deformation or softness in even-even nuclei were found [10,11], including alternating parity bands usually connected by strong electric dipole (E1) transitions. The strength of the observed E1 transitions from states of spin I_i to spin I_f, B(E1:$I_i \rightarrow I_f$), may be converted into an intrinsic electric dipole moment D_0 using a rotational model prescription.

$$\mathrm{B(E1};I_i \rightarrow If) = \frac{3}{4\pi} D_0^2 < I_i 010; I_f 0 >^2 .$$

Figure 7 shows values of this moment for a range of even-even nuclei near mass 150.

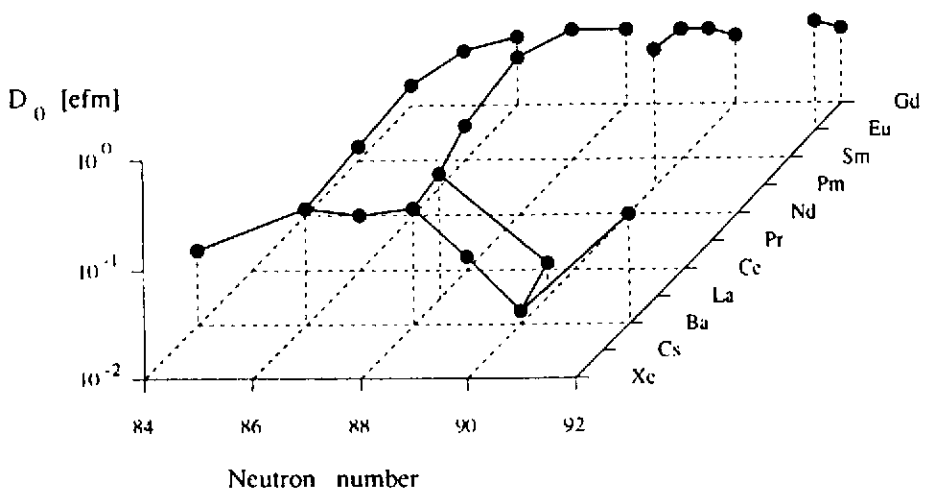

Figure 7. Intrinsic electric dipole moments for nuclei near mass 150.

More conclusive information on the influence of octupole effects can be obtained from studies of odd-A nuclei in this region. In odd-A nuclides, parity doublet bands with similar properties and connected by (usually) strong E1 transitions are expected if the correlations are strong enough to give stable octupole-deformed shapes. Recent experiments on odd-Ba nuclei [12,13,14] have revealed no strong evidence for such parity doublets although strong E1 transitions were observed [14] using spin-parity asignments based on systematics. The moment obtained for ^{143}Ba from the average of the E1 strengths is similar to those observed in ^{142}Ba and ^{144}Ba. No well-developed structures suggestive of reflection-asymmetry are seen in ^{145}Ba, although E1 transitions are observed. Using these to deduce an intrinsic E1 moment produces a value somewhat smaller than that observed in ^{143}Ba and ^{144}Ba and confirms the theoretical predictions of a downward trend towards ^{146}Ba.

A summary of the situation in the odd-A Ba isotopes is that features expected for reflection-asymmetric odd-A nuclei, such as parity-doublet bands, have not been observed in a clearly-developed form, even though the intrinsic electric dipole moments in these nuclei as determined from a rotational model follow the same trend as seen in the even-even isotopes, a trend reproduced by reflection-asymmetric model calculations [16]. In contrast, odd-proton nuclei in this region, such as ^{151}Pm and ^{153}Eu , show [17,18] extended opposite-parity band structures connected by strong E1 transitions. However, these bands exhibit different magnetic properties suggesting a reflection-symmetric rather than asymmetric description.The odd-A La isotopes studied [19] in the EUROGAM2 experiments with ^{248}Cm show no clearly defined parity-band strucures although the E1 strengths measured determine an intrinsic E1 moment of size similar to those observed in the other odd-Z nuclei. A reason for the different behaviour observed in odd-N and odd-Z nuclei in this region may be different blocking effects for neutrons and protons.

4.2 Shape trends in the mass 100 region–lifetime measurements

As the neutron number in Sr and Zr isotopes increases through 60 there is a well-known rapid change of ground-state shape to large deformation, with these nuclei exhibiting [6] good rotational features. We have now measured [20] the lifetimes of higher-lying members of the ground-state bands of ^{98}Sr and of even-even Zr and Mo isotopes in order to investigate the stability of the deformation with rotation. The measured lifetimes have been transformed into quadrupole moments within a rotational model description. The present results, which correspond to a fit to the lineshapes of γ rays from the decay of the J=8, 10 and 12 members of the ground-state bands, are given in the final column of the table below. The column labelled Raman shows the values of the quadrupole moment derived[21] from the lifetimes of 2^+ states; that labelled Moller shows theoretical predictions[22] of ground-state moments. It can be seen that the new data strongly suggest that the shapes of the well-deformed Sr and Zr nuclei do not change with angular momentum, at least up to spin $12\hbar$. This is consistent with theoretical expectations from calculations[22] of Total Routhian Surfaces (TRS).

Nucleus	Raman	Moller	Present
^{98}Sr	3.12(18)	3.14	3.17(20)
^{100}Zr	3.01(19)	3.36	3.19(10)
^{102}Zr	4.01(40)	3.51	3.52(17)
^{104}Zr		3.68	3.72(16)
^{102}Mo	3.26(19)	3.29	2.44(17)
^{104}Mo	3.29(13)	3.54	2.84(14)
^{106}Mo	3.62(10)	3.70	2.85(13)
^{108}Mo	3.58(42)	3.46	2.79(20)

In contrast to the rigidity of the Sr and Zr isotopes, there is a consistent reduction of 20% in the quadrupole moments of the intermediate spin states in the Mo isotopes as spin increases. This is also predicted by TRS calculations which suggest that, as the nuclei rotate, the yrast states take on a triaxial shape due to the alignment of $h_{\frac{11}{2}}$ neutrons. The tendency to triaxiality in the Mo isotopes is of interest, because the Ru isotopes exhibit [23] characteristics of rigid triaxiality. Thus more detailed information on the transition from axial symmetry in the Sr and Zr isotopes to rigid triaxiality in Ru, via the Mo isotopes

could clarify the role of different deformed orbitals in that evolution.

4.3 Two-phonon vibrational states

Rotational bands based on intrinsic structures in deformed nuclei which correspond macroscopically to vibrations about simple average shapes are well established. One such is the gamma vibrational band based on a triaxial oscillation of a nuclear shape which on average has axial symmetry. Levels with positive parity and spin quantum number 2 have an intrisic stucture corresponding to one phonon of such a vibration. Regular searches have been made for good candidates for levels which correspond to two phonons of gamma vibration, and recently[24] data from fission gamma rays have suggested that the neutron-rich Mo and Ru nuclei may provide excellent candidates.

Figure 8 shows the level scheme obtained for ^{106}Mo from the EUROGAM2 experiments with ^{248}Cm. The level at 1435 keV excitation energy is below the pairing gap which is close to 2 MeV and hence the level has a strongly collective nature; it has an excitation energy twice that of the level at 710 keV which has an internal structure corresponding to one phonon of gamma vibration. The 1435 keV state has spin quantum number 4 and positive parity as required for a state corresponding to two gamma-phonons. The decay properties of the band based on the 1435 keV state are also consistent with such a description, and the 1435 keV state is one of the best candidates known for a state with two quanta of gamma-vibration.

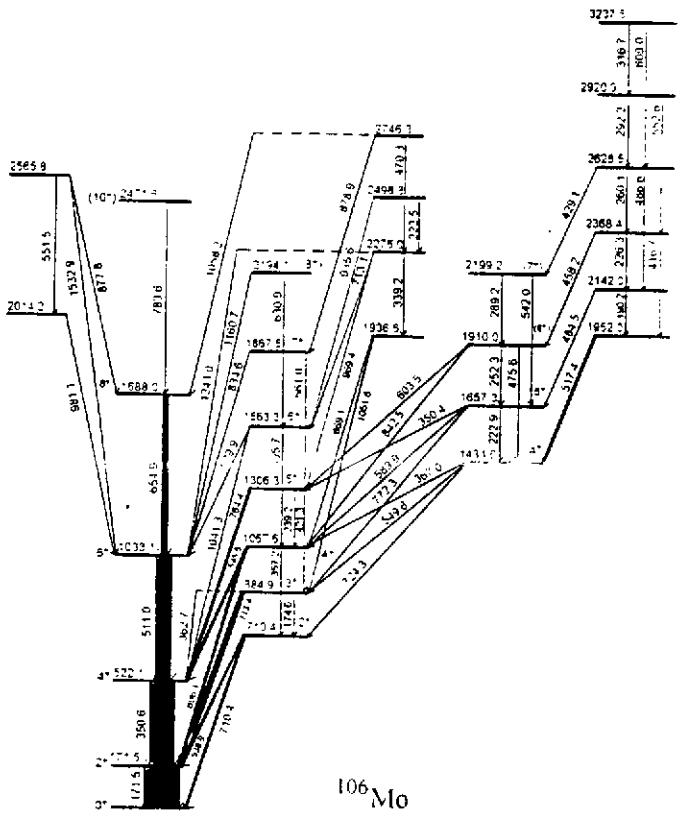

Figure 8. A partial decay scheme for ^{106}Mo.

The work discussed in this paper has been performed in collaboration with several researchers from the University of Manchester, the Argonne National Laboratory, USA, and the CNRS Laboratory at Strasbourg. For several of the topics outlined in this paper special thanks are due to M.A.Jones, W.Urban, A.G.Smith and N.Schulz. The work was supported by the Science and Engineering Research Council of the UK under grant no. GRH71161, and by the US Dept. of Energy under contract No. W-31-109-ENG-38. The author is also indebted for the use in experiments of ^{248}Cm to the Office of Basic Energy Sciences, US Dept. of Energy, through the transplutonium element production facilities at the Oak Ridge National Laboratory.

References

1) B.F.Rider, Vallecitos Nuclear Center Report No. NEDO-12154-3(B), 1980
2) K.F.Flynn *et al.*, J.Inorg. Chem. 37 (1975) 881-5
3) R.W.Peele and F.C.Maienschein, Phys. Rev. C3 (1971) 373-90
4) V.V.Verbinsky *et al.*, Phys. Rev. C7 (1973) 1173-85
5) Y.Abdelrahman *et al.*, Phys. Lett. 199B (1987) 504-8
6) M.A.C.Hotchkis *et al.*, Nucl.Phys. A530 (1991) 111-34
7) I.Ahmad and W.R.Phillips, Rep. Prog. Phys. 58 (1995) 1415-63
8) R.M.Steffen and K.Alder, in The Electromagnetic Interaction in Nuclear Spectroscopy, ed. W.D.Hamilton (North-Holland, 1975)
9) A.G.Smith *et al.*, Phys. Rev. Lett. 73 (1994) 2540-2
10) W.R.Phillips *et al.*, Phys. Rev. Lett. 57 (1986) 3257-9
11) W.R.Phillips *et al.*, Phys. Lett B212 (1988) 402-6
12) J.D.Robertson *et al.*, Phys. Rev. C34 (1986) 1012-1023
13) J.D.Robertson *et al.*, Phys. Rev. C40 (1989) 2804-2822
14) S.J.Zhu *et al.*, Phys. Lett. B357 (1995) 273-80
15) M.A.Jones *et al.*, Nucl. Phys. A605 (1996) 133-43
16) P.A.Butler and W.Nazarewicz, Nucl. Phys. A533 (1991) 249-61
17) W.Urban *et al.*, Phys. Lett. B247 (1990) 238-41
18) C.J.Pearson *et al.*, Phys. Rev. C49 (1994) 1239-42
19) W.Urban *et al.* Phys. Rev. C54 (1996) 945-8
20) A.G.Smith *et al.*, Phys. Rev. Lett. 77 (1996) 1711-1714
21) S.Raman *et al.*, At. Dat. Nucl. Dat. Tables 36 (1987) 1-96
22) P.Moller *et al.*, At. Dat. Nucl. Dat. Tables 59 (1995) 185-382
23) J.A.Shannon *et al.*, Phys. Lett. B336 (1994) 136-40
24) A.Guessous *et al.*, Phys. Rev. Lett. 75 (1995) 2280-2283